Cytokinetic abscission dynamics in neuroepithelial stem cells during brain development

Katrina C. McNeely[1,2], Jessica Neville Little[1,3], and Noelle D. Dwyer[1*]

[1]Department of Cell Biology, [2]Neuroscience Graduate Program, and [3]Medical Scientist Training Program, University of Virginia School of Medicine, Charlottesville, VA 22908, USA *Correspondence: ndwyer@virginia.edu

Running Title

Abscission in NESCs of developing brain

Keywords

Cytokinesis, Midbody, Microcephaly, Mouse, Stem Cell, Cerebral Cortex

Abstract

While mechanisms of cytokinesis have been identified in single cell models, the spatial and temporal regulation in developing tissues is less understood. Here we compare cytokinetic furrowing and abscission in mouse neuroepithelial stem cells (NESCs) at different developmental stages and in a cytokinesis mutant. We image abscission dynamics in this polarized epithelium for the first time. We find that furrows of NESCs ingress asymmetrically at a steady rate, and form the midbody at the apical membrane. Abscission is usually observed on each midbody flank, releasing the midbody remnant onto the apical surface. Interestingly, midbody remnants are more associated with early proliferative divisions. In the microcephalic *Kif20b* mutant, NESC abscission is accelerated, and daughter cells show increased cell cycle exit that is p53-independent. These results suggest that abscission in stem cells is developmentally regulated to influence daughter cell fates and ensure proper brain growth and structure.

Introduction

Regulation of cytokinesis is essential for the formation of every tissue in the body. However, the roles of cytokinesis in the stem cells that produce daughter cells in a specified order to build multicellular tissues have only begun to be addressed. In particular, the temporal and spatial regulation of cytokinetic abscission in stem cells may influence the balance of proliferation, differentiation, and daughter fates, but it remains poorly understood.

The basic mechanisms of cytokinetic furrowing and abscission have been established primarily from studies in single cell models (Green et al., 2012; Herszterg et al., 2014; Nahse et al., 2017). After chromosome segregation, cleavage furrow ingression compacts the central spindle microtubules into a structure called the midbody (MB) within the intercellular bridge. The MB contains > 150 proteins that assemble into domains including a central bulge and lateral flanks (Mierzwa and Gerlich, 2014; Skop et al., 2004). Abscission, severing of the intercellular bridge, occurs when MB microtubules are disassembled at constriction sites on the MB flanks, coincident with plasma membrane scission (Connell et al., 2009; Guizetti et al., 2011). Evidence from developing worms and flies, as well as mammalian stem cell lines, suggests that temporal and spatial regulation of abscission can influence cell polarity and fate (Dionne et al., 2015; Ettinger et al., 2011; Kuo et al., 2011; Lenhart and DiNardo, 2015; Pollarolo et al., 2011; Salzmann et al., 2014; Singh and Pohl, 2014). In cancer-derived cell lines, phagocytosis of MB remnants promotes proliferation (Peterman et al., 2019). More

study is needed to understand how these cytokinetic mechanisms are regulated in stem cells to build tissues such as the brain.

Neuroepithelial stem cells (NESCs) of the cerebral cortex appear to be especially vulnerable to perturbations in cytokinesis, perhaps because they must maintain the pseudostratified epithelial structure and produce billions of neurons and glia in a short time. Indeed, mouse and human mutations in genes encoding MB proteins cause lethal microcephaly (Bondeson et al., 2017; Di Cunto et al., 2000; Frosk et al., 2017; Janisch et al., 2013; Li et al., 2016). NESCs are highly polarized, with apical endfeet that line the lateral ventricle, and long basal processes that contact the pia. Their nuclei move to the apical membrane for mitosis and cytokinesis. At first, NESCs perform symmetric proliferative divisions to produce two NESC daughters and expand the epithelium. Later, NESCs increase neurogenic divisions, producing neuron daughters that exit the cell cycle, detach their apical junctions, and migrate basally (Bizzotto and Francis, 2015; Dwyer et al., 2016). The mechanisms that change from proliferative to neurogenic divisions remain poorly understood. Candidate fate determinants include apical components that are segregated during cytokinesis, such as apical junctions, Notch/Numb, centrosomes, and the MB itself (Dubreuil et al., 2007; Higashi et al., 2016; Kim et al., 2010; Paridaen and Huttner, 2014).

Previously, we showed that mutation of the Kinesin-6 *Kif20b* in mice causes microcephaly (Dwyer et al., 2011; Janisch et al., 2013). Kif20b localizes to the central spindle during furrowing, then to MB flanks and constriction sites (Abaza et al., 2003; Janisch et al., 2018). We showed in HeLa cells, Kif20b depletion disrupts furrowing speed, MB maturation and abscission timing, but not completion (Janisch et al., 2018).

This raised the question of whether Kif20b loss in NESCs causes similarly subtle or more severe defects in cytokinesis, possibly contributing to the microcephaly phenotype. In fixed brains of *Kif20b* mutants, we found no changes in mitotic or S-phase indices of cortical NESCs. Interestingly, the cortical NESCs did have a reduced midbody index and wider, disorganized MBs, but no increase in binucleate cells, which suggested a specific abscission defect. NESC apoptosis was elevated in the mutant embryo brains, suggesting that abscission defects cause apoptosis in a fraction of NESCs. We later found through a genetic cross of Kif20b with the p53 deletion mutant, that p53 loss fully blocks the apoptosis, but does not block the midbody defects, and only partially rescues the microcephaly. These findings suggested that Kif20b loss and abscission defects could lead to other consequences for NESCs aside from apoptosis, that could account for the remaining microcephaly (Janisch et al., 2013; Little and Dwyer, 2019). Therefore, we wanted to more precisely define Kif20b's role in cytokinesis of NESCs, and test for other NESC daughter cell fate changes.

Here we address how cytokinetic mechanisms are regulated in neural stem cells during brain development. We perform for the first time, quantitative analysis of cytokinetic furrow ingression and abscission in NESCs through live imaging in intact cortical explants. We compare different developmental stages of control and *Kif20b* mutant brains. Our data suggest that abscission timing and MB disposal are regulated differently in proliferative and neurogenic NESC divisions. Bilateral abscission is frequently observed, releasing the midbody remnant (MBR) at the ventricular surface, consistent with the idea that the MBR has cell to cell signaling potential. Furthermore, in the *Kif20b* mutant NESCs, abscission is accelerated, and daughter cells are more likely

to exit the cell cycle to become neurons. Thus the severe microcephaly caused by the loss of Kif20b can be attributed to early depletion of NESCs through two mechanisms: p53-dependent apoptosis and p53-independent cell cycle exit. Together these data add to a growing body of work showing that abscission timing and MBRs can influence stem cell daughter fates and tissue development.

Results and Discussion

Asymmetric cytokinesis in cortical NESCs

Cortical NESCs furrow asymmetrically, from basal to apical, and form the MB at the apical membrane (Fig 1A, A'). This may help maintain the polarity and apical adhesions of the stem cell niche. However, furrow ingression kinetics have not been analyzed in this system, in normal brains or cytokinesis mutants. To measure furrowing kinetics in NESCs within the polarized neuroepithelium, we adapted our previously established fixed cortical slab explant method (Janisch and Dwyer, 2016). Dissecting cortices from membrane-GFP transgenic mice, and labeling polymerized microtubules with SiR-Tubulin, enables live time-lapse imaging of NESC cytokinesis from the apical surface. After the NESC apical endfoot rounds up in mitosis, the furrow initiates on the basal side, and ingresses asymmetrically towards the apical membrane as a contractile arch, rather than a ring (Fig 1B, C). In both E11.5 and E13.5 control cells, ingression proceeds smoothly, at a constant rate, over ~15 minutes until completion (Fig 1D-F, S1A-C). Most *Kif20b -/-* NESCs behave like controls, and none show furrow regression. However, a subset furrow abnormally, taking 24 minutes to complete (Fig 1C-F, Fig S1C). Previously, we showed acute depletion of Kif20b in HeLa cells did not prevent

furrow completion, but slightly reduced ingression rate (Janisch et al., 2018). Thus, our HeLa cell data predicted a subtle *Kif20b* mutant NESC furrowing defect, but also highlight the need for more studies to elucidate how polarized cytokinesis in epithelial stem cells is mediated.

Abscission duration is variable in NESCs and regulated by Kif20b

Mammalian cell lines such as HeLa and MDCK have been used to model mechanisms and kinetics of cytokinetic abscission, but it is unclear whether these immortalized cells accurately model abscission dynamics in tissue stem cells that must balance proliferation with differentiation. Using the cortical explant culture method, we analyzed the spatial and temporal dynamics of abscission in NESC MBs at the apical membrane. We defined abscission as microtubule disassembly on a MB flank, observed as the tubulin signal intensity at the abscission site decreasing to background level. Figure 2A shows a representative NESC at an early stage of abscission, with a wide MB. A rotated image stack (X-Z view) illustrates how the MB bridges the two daughter cells across their cell junction. At later stages of abscission (Fig 2B), the MB is thinner, and sometimes a microtubule constriction site can be seen on one flank. Time-lapse imaging captures the steps of abscission (Fig 2C, D).

To ask if abscission duration changes as brain development proceeds and NESC divisions switch from proliferative to neurogenic, we measured the time from MB formation to first abscission at two different ages. We found that the duration ranged from 15 to 120 minutes, with means of 57 and 47 minutes at E11.5 and E13.5, respectively (Fig 2E, F). A cumulative frequency plot shows a trend to faster abscission

at the later age, when divisions are more frequently asymmetric and neurogenic (Fig 2G, solid lines).

We previously found that fixed *Kif20b* mutant embryo brains display misshapen and disorganized MBs, and that Kif20b-depleted HeLa cells have dysregulated abscission timing. These data predicted that some *Kif20b* mutant NESCs have delayed or failed abscissions. To our surprise, in live imaging, every mutant NESC observed was able to complete abscission. Remarkably, the average time to first abscission was reduced compared to controls, by 18 minutes at E11.5, and 9 minutes at E13.5 (Fig 2E, F). Moreover, the cumulative frequency plot of *Kif20b* mutant abscissions shows similar curves at the two ages, suggesting a loss of developmental regulation (Fig 2G, dashed lines). Also, at E13.5, *Kif20b* mutant MBs appear to be wider at the last time point captured before abscission, suggesting they abscise prematurely, or they narrow more rapidly than controls (Fig S1D, E). These data are consistent with our prior findings in fixed samples that *Kif20b* -/- NESC MBs tend to be wider than controls' (Janisch et al., 2013; Little and Dwyer, 2019). Together these data support the idea that Kif20b function is important in early NESCs to coordinate abscission timing with MB maturation. The consequences of premature abscission for stem cell polarity or fate are unknown.

Next, we wanted to determine the frequency of cortical NESCs abscission on one or both MB flanks, the relative timing, and if this varies with developmental stage. Some studies in HeLa, fly germline, and *C. elegans* embryos reported MB abscission on one flank and inheritance by the opposite daughter (Daniel et al., 2018; Ettinger et al., 2011; Gromley et al., 2005; Kuo et al., 2011; Salzmann et al., 2014; Singh and Pohl, 2014). Other studies, by ourselves and others, report sequential abscissions on each flank in

HeLa, MDCK and *C. elegans* cells (Chai et al., 2012; Gershony et al., 2017; Guizetti et al., 2011; Janisch et al., 2018; Konig et al., 2017; Lafaurie-Janvore et al., 2013).

An attractive hypothesis is that an early symmetric proliferative division of a cortical NESC would occur through bilateral abscission and release of the MBR extracellularly, whereas a later asymmetric neurogenic division could result from unilateral abscission on one flank and MB inheritance by the other daughter, promoting asymmetric fates. Indeed, MBRs have been found in cerebrospinal fluid of early (E10.5) mouse embryos (Dubreuil et al., 2007). However, we detected bilateral abscission just as often in E13.5 divisions as E11.5 divisions, in at least 60% of the cases (Fig 3A, B). The two abscissions usually occurred sequentially, but occasionally took place within the same time interval. The median time between the 1st and 2nd event was 30 minutes at E11.5 and 15 minutes at E13.5, with a maximum of 90 minutes (Fig 3C, D). It is not clear whether the cases where only a single abscission could be scored with confidence were truly unilateral, or whether the second event was not detected due to imaging conditions. Further studies are needed to determine whether bilateral abscissions are a specific feature of proliferative stem cells or symmetric daughter fates.

We also asked whether Kif20b loss alters bilateral abscission frequency or kinetics in NESCs. It does not significantly alter the frequency (Fig 3 A, B), but does significantly reduce the time between first and second abscissions at E11.5 NESCs (Fig 3C). In total, the mean time to complete bilateral abscissions was 23 minutes less in the *Kif20b* mutants at E11.5, and 13 minutes less at E13.5 (Fig 3E, F, G). Thus, Kif20b loss does not prevent MB release, and may in fact hasten it.

Increased association of MBRs with younger proliferative NESC divisions

The release of MBRs at the apical membrane suggests they could impact cell fate and polarization, perhaps by packaging or removing fate determinants. Potentially, MBRs could transmit signals to neighboring cells by surface binding or uptake, as seen in other cell types (Chai et al., 2012; Crowell et al., 2014; Fazeli et al., 2016; Peterman et al., 2019). MBRs were reported to influence ciliogenesis on MCDK cells, proliferation vs differentiation in cell lines, and spindle orientation in *C. elegans*. (Bernabe-Rubio et al., 2016; Ettinger et al., 2011; Kuo et al., 2011; Singh and Pohl, 2014).

We wondered whether NESC MBRs float into the ventricle, or remain associated with the apical membrane. In live explants, we were not able to follow MBRs after the second abscission. So, we used fixed cortical slabs to study MBR disposal at different ages. MBRs can be identified by immunostaining for endogenous Citron kinase (CitK) and Aurora Kinase B (AurKB) (Fig S2)(Ettinger et al., 2011). We quantified MBRs on the apical surface at two ages, when divisions are primarily proliferative (E11.5) or neurogenic (E15.5). Both pre-abscission MBs (brackets) and post-abscission MBRs (arrowheads) are observed at the apical membrane at both ages (Fig 4A). Interestingly, there were ~4-fold more MBRs observed on E11.5 cortices than E15.5 (Fig 4B). This striking difference suggests that E15.5 NESCs may have different regulation of either MBR release or degradation. This developmental difference was not altered by Kif20b loss.

To more precisely quantify MBR association with individual NESC divisions, we modified the established NESC “pair cell” assay (Qian et al., 1998). NESCs were plated as single cells at clonal density, and fixed the next day to score individual NESC

daughter pairs for the presence of MBRs (Fig 4C, D). Similar to the *in vivo* analysis, E11.5 division pairs were ~6-fold more likely to have a MBR present than E15.5 pairs (Fig 4E). Again, Kif20b is not required for this developmental change.

These data suggest that MBRs are more associated with early proliferative NESC divisions than later neurogenic divisions. To test this further, we scored MBR association in the different types of divisions of E11.5 NESCs. By co-labeling with NESC and neuron markers, the division pairs were classified as proliferative symmetric, neurogenic symmetric, or asymmetric (Fig 4F). Interestingly, E11.5 division pairs that have an associated MBR are more likely to be proliferative symmetric (Fig 4G, control). This supports the idea that MBR presence, and perhaps bilateral abscission, are associated with proliferative symmetric division. Curiously, in the *Kif20b* mutant, this association is no longer seen, perhaps due to an overall reduction of proliferative symmetric divisions (Fig 4G, Kif20-/- bars). Thus, MBR presence may influence a NESC division towards proliferative symmetric fates, but does not appear to be the primary effector in this process. It is not known if NESCs have similar mechanisms for MBR engulfment and degradation as other cell types (Chai et al., 2012; Crowell et al., 2014), but differential regulation of these processes in early versus late-stage stem cells could alter the ability of MBRs to influence the polarity or fates of progeny. The composition and signaling capacity of MBRs in stem cells and other dividing cell types require further investigation.

Premature cell cycle exit of early Kif20b mutant NESCs may contribute to microcephaly

We noticed that *Kif20b -/-* NESCs had fewer proliferative symmetric divisions, and more neurogenic divisions than controls, regardless of MBR association (Fig 4G). To directly test whether *Kif20b -/-* NESCs have different division outcomes, we quantified the daughter fates of individual divisions. Pooling division pairs with and without MBRs, we find that *Kif20b* mutant NESCs from E11.5 brains have a significant increase in neurogenic symmetric outcomes compared to controls, 61% versus 42% (Fig 5A). This comes at the expense of fewer proliferative symmetric divisions (17% vs 38%). NESCs from E15.5 brains normally have more neurogenic than proliferative divisions (Fig 5B, control, and Fig S3A). However, *Kif20b* mutants do not show this profound developmental shift (Fig 5A, B Fig S3B). This suggests that Kif20b's function helps maintain stemness, biasing early NESC divisions to produce two NESC daughters.

These data suggest *Kif20b* mutant NESCs have premature neurogenesis (early cell cycle exit). To test this *in vivo,* we measured the width of the earliest neuronal layer (preplate) at E12.5 in control and mutant brains. We find a small but highly significant increase in the proportional thickness of the preplate in *Kif20b -/-* cortices (Fig 5C, D), not due to decreased neuron density (Fig 5E). These results suggest that in early *Kif20b-/-* cortices, some daughters of NESC divisions prematurely exit the cell cycle to become postmitotic neurons. This depletion of the early stem cell pool would reduce the potential brain size at birth.

We previously showed that some NESCs in *Kif20b* mutant cortices undergo apoptosis, and that this is p53-dependent (Little and Dwyer, 2019). We also showed p53 accumulates in the nucleus of *Kif20b -/-* NESCs at late MB stage. Therefore, we

hypothesized that the increased early cell cycle exit could also result from p53 activation. To test this, we assayed division types in *Kif20b; p53* double mutant NESCs. Surprisingly, the increase in symmetric neurogenic divisions caused by loss of Kif20b is not prevented by p53 knockout (Fig S3D). Both the *Kif20b* and *Kif20b; p53* double mutants have a 45% increase in neurogenic divisions. Cell cycle exit was increased in NESCs double mutant for Kif20b and p53, but not p53 alone (Fig S3E). Thus, our data show that early NESCs in the *Kif20b* mutant mouse are depleted due to both p53-dependent apoptosis (Little and Dwyer, 2019) and p53-independent cell cycle exit (this paper).

Recent progress in cell lines has elucidated a few of the signaling molecules that activate p53-mediated cell cycle arrest following mitotic delay, but abscission delay was not addressed (Lambrus et al., 2016; Meitinger et al., 2016). Furthermore, cortical NESC daughters appear to respond differently: p53 is not required for cell cycle exit (neurogenesis) following mitotic delay, but p53 does mediate apoptosis in some cells instead (Pilaz et al., 2016). This echoes the aforementioned findings in *Kif20b* mutant NESCs, but we found no evidence for delayed or defective mitosis in the *Kif20b* mutant (Janisch et al., 2013; Little and Dwyer, 2019). Since cell cycle exit is a normal developmental event for the neuronal daughters of NESCs, a non-p53 pathway may be primed to mediate it. Recent evidence suggests NESCs may be more sensitive to p53 levels than other stem cell types such as cardiac (Bowen et al., 2019). Since stem cells must give rise to many daughters over a long time window, they may have evolved sensitive responses to defects in cell division so they exit the cell cycle or undergo apoptosis rather than produce damaged daughter cells that would disrupt tissue

structure or function. More studies are needed to determine whether and how p53 and other pathways are activated by defects in MB structure or abscission timing.

The consequences of altered abscission timing in stem cells or other cell types are poorly understood (Stoten and Carlton, 2018). Interestingly, delayed abscission timing in the fly germline is important for maintaining stem cell fate (Lenhart and DiNardo, 2015). Delayed abscission in HeLa cells causes persistent intercellular bridges, MB regression/ binucleation, or cell death (Gromley et al., 2003). Faster abscission was induced in HeLa cells, but no morphological or fate consequences were described (Carlton et al., 2012). In cortical NESCs, fate-signaling events at the apical membrane happen concurrently with abscission, and could be affected by abscission duration. These include new apical junction building, notch signaling across it, and centrosome docking/ ciliogenesis. As these events occur, the MBR could accumulate fate determinants to sequester or transmit. Future studies in multiple stem cell types and developing tissue systems are needed to further elucidate how developmental regulation of abscission contributes to stemness, differentiation, and building tissues and organs.

Materials and Methods

Mice

The mouse protocols are approved by the IACUC and the colonies are maintained in accordance with NIH guidelines. The morning of the vaginal plug was considered E0.5. All embryos were harvested by cesarean section and littermate controls were used when possible. The *Kif20b*^{magoo} (*Kif20b*$^{-/.}$) mutant mouse was generated in an ENU

screen (Dwyer et al. 2011). It carries a loss-of-function splice site mutation that reduces the protein to undetectable levels (Janisch et al., 2013). The *Kif20b* mutant mouse was crossed with both the mT/mG reporter line (Jax stock #007576) and Sox2-Cre mice (JAX stock #008454) (Hayashi et al., 2002; Muzumdar et al., 2007) to produce mice that expressed membrane-localized GFP. The p53 null mouse ($Trp53^{tm1Tyj}$ (JAX stock #002101) was crossed to the *Kif20b* mutant mouse (Jacks et al., 1994; Little and Dwyer, 2019).

Antibodies and immunofluorescence staining

Following fixation, cortical slabs or NESC cultures were incubated for an hour at room temperature (20 °C) in blocking buffer (0.1% Triton-X, 2-5% Normal Goat Serum in PBS) and then overnight at 4 °C or for three hours at room temperature (20 °C) in the appropriate primary antibody solution (antibody diluted in blocking solution). After primary incubation, coverslips (Fisher Brand Microscope Coverglass 18Cir-1D Cat #: 12-545-84) were rinsed in PBS (3 times every 10 minutes) or slabs were rinsed in PBS-triton once followed by two PBS rinses and then incubated at room temperature (20 °C) with appropriate secondary antibody solution (1:200 dilution) for 30 minutes (cultures) or 45 minutes (slabs) in the dark. Following final washes in PBS, coverslips were mounted onto glass slides with flurogel (Electron Microscopy Sciences 17985-10) or slabs were cover-slipped (22 x 22 #1 cover glass, Curtin Matheson Scientific Inc Cat #: 089-409) with Fluoromount (Vectashield, 4-1000). Antibodies used: Nestin (Aves Lab, NES), Tubb3 (TUJ1, Abcam rabbit 52623, Biolegend mouse 801201), Citron kinase (CITK, BD Biosciences 611376), Aurora B (AurKB, Abcam ab2254), Phalloidin (ThermoFisher

A12380), Cep55 (Santa Cruz sc-377018), Survivin (Cell Signaling Technology 2808), BrdU (BD Biosciences 347580).

Pair cell assay and NESC cultures

The pair cell assay for dissociated cortical NESC divisions was adapted from (Chau et al., 2015; Qian et al., 1998). E11.5, E12.5 or E15.5 mouse embryos were dissected from the dam in hibernate media (Gibco Hibernate-E A12476-01). Cortices were removed and placed into a 15 mL conical tube. Meninges were removed from E15.5 cortices. Papain from Worthington kit (Worthington Biochemical Corporation, LK003150) was used for dissociation. Cortices were placed on a rotator at 37 °C for 30 minutes (E11.5 or E12.5) or 45 minutes (E15.5). Manual dissociation followed by centrifugation at 4 °C at 1300 rpm for 10 minutes and then wash with DMEM (Invitrogen 11960-051). The wash and centrifugation are repeated three times. After the final wash, the cortices were manually dissociated with a 1 mL pipette followed by a glass Pasteur pipette. The tissue was resuspended in final culture media (resuspension volume varied by age and size of cortices). Final culture media is base media filtered with 0.22 µm cellulose acetate membrane (BD Biosciences 302995) with 100 µL of 100X N2 (Invitrogen Cat. No. 17502-048) and 100 µL 100X N-acetyl-cysteine (Sigma Cat No A-9165), and 20 µL of 10 µg/mL bFGF (Invitrogen Cat. No. 13256-029) per 20 mL. Base media is DMEM with 2 mL100X Na-Pyruvate (Invitrogen 11360–070), 2 mL 200 nM L-glutamine (Gibco A2916801), 4 mL 50X B-27 without Vitamin B (Gibco 12587010) per 200 mL of DMEM. The cortices were at room temperature (20 °C) for 15 minutes to allow for the clumps to settle to the bottom of the conical tube. Between 1 to 3 µL of cells from the top of the tube were added to each well of the poly-L-lysine coated Terasaki plates (Fisher cat #

07-000-401) to get a low density. The plates were placed in a humidifying chamber and into a 37 °C incubator with 5% CO_2 to incubate for 20 hours. NESC cultures were fixed with 4% paraformaldehyde (PFA) for 2 minutes followed by 5 minutes cold methanol (100% methanol at -20 °C) in -20 °C freezer. Immunostaining was followed as described above except the plate was kept in a humidified chamber to prevent evaporation and volumes of washes and antibodies were adjusted. All washes were done by flooding the plate with 5 mL of PBS. Primary and secondary incubations were done by adding 10 µL of solution to each well.

Images were acquired using a Zeiss AxioZoom Observer.Z1 with a 40x air objective.

BrdU in a modified pair cell assay

We modified the previous assay by feeding BrdU to higher density NESC cultures at plating, so that NESCs that divided in the dish could be identified as BrdU+ pairs. Primary cortical NESCs were plated on coverslips at 100,000 cell density with 10 µM BrdU (Sigma B5002-500mg) and allowed to incubate at 37 °C for 6 hours. The media was exchanged to wash out the BrdU, and the culture continued to incubate for 14 hours. The cells were then fixed at 20 hours with 4% PFA for 10 minutes. Antigen retrieval was performed using 0.07 M NaOH for 2 minutes before proceeding to immunostaining. Images were acquired at 40x using a Zeiss AxioImagerZ1 microscope with AxioCam mRM.

Cortical slabs for fixed tissue

This method was previously described (Janisch and Dwyer, 2016). Briefly, the skulls were opened to reveal the cortices. The entire head was fixed for 20 minutes in 2% PFA for E11.5 and 4% PFA for E15.5. Cortices were pinched off and placed in slide wells

(Cat # 70366-12, 70366-13). The total slab thickness varied by age (E11.5: ~150μm, E15.5: ~400μm). The slabs were briefly fixed again with PFA before immunostaining. Images were acquired using the 60x objective on the Applied Precision (GE) DeltaVision microscope. E11.5 or E15.5 cortical slabs were immunostained for the endogenous MBR marker citron kinase (CitK) and flank marker AuroraB (AurKB) to analyze the number and location of midbodies and midbody remnants. Pre-abscission midbodies were identified by CitK in the bulge surrounded by two AurKB positive flanks. Post-abscission midbody remnants were identified by the shape (ring or oval) and size (not greater than 1.5 μm diameter) of the CitK.

Cortical slabs for cleavage furrow and abscission live imaging

E11.5 or E13.5 embryos were removed from the uterus and dissected in cold 1x PBS. Embryos were checked for GFP or RFP fluorescence before removal of cortices. The embryos heads were removed followed by the opening of the skull. Once the skull had been opened tweezers were used to pinch out the cortices. Each cortex was placed into a glass bottom dish (MatTek P35G-1.0-20-C) with 50 nM silicone-rhodamine tubulin (SirTubulin) (Cytoskeleton CY-SC002) made in final culture media. The slabs were then trimmed and flipped, so the apical surface was facing towards the glass coverslip. Each dish was placed in a humidifying chamber and into a 37 °C incubator with 5% CO_2 overnight (Approximately 15 hours). The next day the cortices were removed from the incubator, and the 5 0nM Sir-Tubulin-containing media was removed. Matrigel (Corning 356237) (1:3 dilution in final culture media) was added to the cortical slab. High vacuum grease (Fisher 14-635-5D) was placed on the edge of the glass coverslip, and a

coverslip (Fisher 12-545-100) was placed over the top of the slab. Gentle pressure was applied to the coverslip at the spots where the vacuum grease was placed. The slabs were placed back into the incubator, and the Matrigel was allowed to solidify for 5 minutes. Final culture media was added to the dish, and then imaging was performed. An Applied Precision (GE) DeltaVision with Truelight Deconvolution and softWorx suite 5.5 image acquisition software equipped with a heating plate and 40X objective was used for time-lapse image acquisition. Images were taken every 15 minutes for abscission and every 3 minutes for cleavage furrowing for up to 6 hours. Z steps were 0.4 μm, and approximately 10 μm of the cortical slab was imaged. The total slab thickness varied by age (E11.5: ~150μm, E13.5: ~200μm).

Abscission and cleavage furrow analysis

Deconvolved full-z-stacks and maximum intensity projection images were analyzed using ImageJ. The time zero was MB formation as ascertained by SiR-Tubulin appearance. Abscission was determined as the time point where there was complete removal of tubulin, when the tubulin signal intensity at the abscission site decreased to background level, on one or both sides of the MB bulge. MB membrane scission was shown to be temporally coincident with microtubule disassembly by (Elia et al., 2011; Lafaurie-Janvore et al., 2013; Steigemann et al., 2009), but we cannot rule out that the MB plasma membrane remains connected for some time after the microtubules are gone. The width of the MB was measured at the time point before abscission and was measured on the side of the MB bulge in which abscission occurs. For cleavage furrowing, the length and width of the cell were measured from the time point right before the first ingression of the membrane started. Time zero is the last time point

before furrowing begins. This measurement was done at every time point until (1) the membrane between sister cells appeared continuous and (2) at subsequent time points there was no more narrowing of the furrow edges. Furrowing was then determined to be completed. Images for 3-D renderings were acquired using higher resolution (40x objective, 0.2 μm z-step) image stacks on E13.5 cortical slabs incubated in 200 nM SiR-Tubulin. 3-D renderings were created in Volocity (access to Volocity kindly provided by Dr. Barry Hinton).

Statistical analysis

All data and statistical analysis were performed with Excel (Microsoft) and GraphPad Prism. All error bars are standard error of the mean (s.e.m.). Data were tested for normality. All statistical tests were Student's t-test unless otherwise noted in the corresponding figure or figure legends. χ^2 (chi square) is for population test. Fishers Exact is for individual groups. Statistics for distributions: Kolmogorov–Smirnov (K-S) and Mann-Whitney (M-W) tests. ****p<0.0001, ***p<0.001, **p<0.01, *p<0.05, n.s. not significant:

Online supplement:

Supplemental Figure S1 shows cleavage furrowing at E11 and midbody width right before abscission. Supplemental Figure S2 shows that citron kinase localizes to the midbody bulge and remnant with Cep55. Supplemental Figure S3 shows the cell fate changes observed in the *Kif20b* mutants are p53-independent.

Acknowledgments

This work was supported by NIH (R01 NS076640 and R21 NS106162 to NDD) and the Robert R. Wagner Fellowship to KCM. We thank Xiaowei Lu, Bettina Winckler, Ann Sutherland, Sarah Siegrist, Jung-Bum Shin, Ahna Skop, Maria Lehtinen, Anthony Lamantia and their labs for advice and discussion. We thank Sara Martin and Adriana Ehlers for data analysis.

Author Contributions

KCM conceptualized and performed experiments, curated data for Fig 1-5 and Fig S1-S2, S3 A-B, wrote the first draft, and edited the manuscript. JNL performed and curated data for Fig S3 C-E. NDD conceptualized and supervised experiments, and edited the manuscript.

The authors declare no completing interests.

Figure 1: Asymmetric furrow ingression in control and *Kif20b* mutant NESCs.

(A, A') Schematics of furrow ingression of cortical NESCs as viewed from lateral or apical perspective.

(B) A furrow ingresses from basal to apical in an E13.5 cortical NESC (membrane-GFP, white). "Lateral view" (x-z) is rotated orthogonally from the imaging plane (x-y).

(C) Representative images of furrowing in one E13.5 control and two *Kif20b* mutant (-/-) NESCs. Brackets show furrow width. Furrowing was considered complete when the membrane between sister cells appeared continuous, and there was no additional narrowing of furrow width.

(D) Furrow ingression and (E) pole to pole elongation proceed smoothly in E13.5 control and *Kif20b-/-* cells. Red line: *Kif20b-/-* example 24-min cell shown in C.

(F) Median (blue and red lines) furrow duration is increased in *Kif20b-/-* mutants, with a subset of slower NESCs.

n=25 control cells (from 2 +/- and 1 +/+ brains), and 27 *Kif20b-/-* cells from 3 brains.

Figure 2: Abscission in NESCs is variable in duration but accelerated in *Kif20b* mutant brains.

(A, B) 3D renderings of NESCs at early or late MB stages from both the apical view (imaging plane) and rotated lateral view. MBs (m, arrow) form at apical membrane (ventricular surface). Late MB has constriction site on one flank (arrowhead). L, longitudinal microtubules.

(C, D) Images and schematic of NESC MB undergoing abscission steps: MB formation (m), Microtubule cut 1 (yellow arrowhead), constriction site thinning (white arrowhead) and Microtubule cut 2 (red arrowhead).

(E, F) Time from MB formation to 1st abscission is reduced in *Kif20b* -/- NESCs at E11.5 and E13.5. Red and blue lines show means.

(G) Cumulative frequency plots suggest that E11.5 *Kif20b -/-* NESCs behave like E13.5. For E11.5, n= 46 +/+ cells (from 4 brains); 69 *Kif20b*-/- cells (4 brains). For E13.5, n= 63 +/+ cells (5 brains); 47 -/- cells (3 brains).

Figure 3: Sequential bilateral abscissions are observed in most NESC divisions, and occur faster in *Kif20b* -/- brains.

(A, B) The 2nd abscission was observable in more than 60% of cells in E11.5 and E13.5, regardless of genotype.

(C, D) The 2nd abscission was usually detected within 30 minutes of the first, but within 15 minutes in E11.5 *Kif20b* -/- cells

(E, F) Total time for bilateral abscissions is reduced in *Kif20b* mutants at both ages. Red and blue lines show means.

(G) Cumulative frequency curves of 2nd abscissions suggest E11.5 *Kif20b -/-* NESCs behave like E13.5.

For E11.5, n= 34 +/+ (4 brains); 56 *Kif20b-/-* cells (4 brains). For E13.5, n= 41 +/+ (5 brains); 32 *-/-* cells (3 brains).

Fisher's Exact test for A, B.

Figure 4: Post-abscission midbody remnants (MBR) are detected at the apical membrane, and associated with early proliferative symmetric divisions.

(A-A') Schematic and three image-planes of a field of apical membrane of an E11.5 cortex show many NESC junctions (actin, white), a late furrow in Z1-2 (asterisks), pre-abscission MBs (brackets, A'), and post-abscission MBRs in Z2-3 (arrowheads, A').

(B) Many more MBRs are seen on E11.5 apical membranes than E15.5, normalized to either cell or MB number.

For E11.5, n= 4 control (3 +/- and 1 +/+); 4 *Kif20b*-/- brains. For E15.5, n= 3 control (1 +/- and 2 +/+); 4 -/- brains.

(C) Schematic of pair-cell assay.

(D) Pair of daughters of an E11.5 NESC division *in vitro*, with an associated MBR labeled by CitK (arrowhead).

(E) E11.5 NESC division pairs are more likely to have a MBR present than E15.5 division pairs. This difference does not depend on Kif20b.

(F) Three division types with MBR (Crik+) detected. P, progenitor (Nestin+); N, neuron (Tubb3+); T, transitional neuron (Nestin+, Tubb3+).

(G) The proportions of division types were compared in pairs with or without MBR. Control NESC division pairs with MBRs are more often proliferative, but *Kif20b* -/- NESCs are not.

For E11.5, n= 394 control (3 +/- ,2 +/+ brains); 272 *Kif20b*-/- divisions (4 brains). For E15.5, n= 241 control (4 +/-, 1 +/+ brains); 280 *Kif20b*-/- divisions (5 brains). Fisher's exact test in D, F; χ^2 test in F.

Figure 5: *Kif20b* -/- NESCs show reduced proliferative symmetric divisions and increased neuron daughters in early corticogenesis.

(A, B) *Kif20b* -/- NESCs have less than half as many proliferative symmetric divisions as controls at E11.5, with a concomitant increase in neurogenic symmetric divisions. E15.5 *Kif20b* -/- NESCs show similar percentage as control.

For E11.5, n= 394 control (3 +/- and 2 +/+ brains); 272 *Kif20b-/-* divisions (4 brains). For E15.5, n= 241 control (4 +/- and 1 +/+ brains); 280 *Kif20b-/-* divisions (5 brains).

(C) Sections of control and *Kif20b*-/- E12.5 brains stained for Tubb3 show the nascent neuron layer (preplate, pp) above the NESC nuclei (ventricular zone, vz). The neurons were born from NESC divisions at E11.5.

(D, E) The preplate is proportionally thicker in E12.5 *Kif20b* -/- cortices, but density is similar.

N= 6 control (+/+), 5 mutant (-/-) brains.

χ^2 and Fisher's exact test in B and C

Supplemental Figure 1: Supplemental analyses of furrowing kinetics at E11.5 and midbody width at abscission

(A, B) Furrow width and pole to pole elongation plotted over time shows ingression proceeds smoothly at the same slow rate in both E11.5 control and *Kif20b-/-* cortical slab explants. Red line is one *Kif20b-/-* NESC that took 24 minutes to furrow.

(C) Median (blue and red lines) time to furrow completion was increased in E11.5 *Kif20b* mutant cortices with a subset of NESCs taking 24 minutes to complete.

n=43 control cells from 2 brains (1 +/- and 1 +/+), and 35 *Kif20b-/-* cells from 2 brains.

(D, E) Midbodies appear slightly wider at the time point before 1st abscission in *Kif20b* -/- NESCs at E13.5. Red and blue lines indicate medians.

For E11.5, n= 46 control cells (from 4 +/+ brains); 69 *Kif20b*-/- cells (4 brains). For E13.5, n= 63 control cells (5 +/+ brains); 47 *Kif20b*-/- cells (3 brains).

***p<0.001, **p<0.01, *p<0.05: Student's t-test for C, Kolmogorov–Smirnov (K-S) and Mann-Whitney (M-W) tests for F and G.

Supplemental Figure 2: NESC midbody remnants (MBRs) are marked by Citron Kinase (CitK) and Cep55.

(A) Dissociated E12.5 NESCs identified by endogenous staining for Nestin. Survivin shows two daughter cells still connected by a MB (yellow arrow). CitK appears as a ring around the bulge of MBs(A') and MBRs (white arrows, A'', A'''(Ettinger et al., 2011; Gruneberg et al., 2006)). (B) Images of dissociated E11.5 NESCs immunostained for endogenous CitK, Cep55, and AurKB show their localizations at different midbody maturation stages. AurKB localizes to the flanks of early and late MBs, but is mostly absent in MBRs. CitK localizes as a ring around the bulge of early and late MBs as well as MBRs. Cep55 also accumulates in a ring around the MB bulge, but only at late stages, and remains in MBRs (Bastos and Barr, 2010; Crowell et al., 2014; Kuo et al., 2011). (C) Most MBRs are co-labeled with both Cep55 and Citk.

Scalebars: 5 μm in A; 1 μm in A', A"", and B.

n= 61 control MBR (1 brain), 49 *Kif20b-/-* MBR (1 brain) n.s: Fisher's exact test

Supplemental Figure 3: The increased neuronal fate of *Kif20b* mutant NESC daughters during early cortical development is not p53-dependent.

(A, B) Comparing the proportions of division types in the pair-cell assay between E11.5 and E15.5 NESCs (using the same data set as in Figure 5 A, B) shows that control NESCs have ~4-fold more proliferative symmetric divisions at E11.5 than E15.5, while *Kif20b* mutant NESCs have the same proportion of proliferative divisions at both ages. For E11.5, n= 394 control (3 +/- and 2 +/+ brains) and 272 *Kif20b-/-* divisions (4 brains). For E15.5, n= 241 control (4 +/- and 1 +/+ brains) and 280 *Kif20b-/-* divisions (5 brains). (C) Higher density dissociated NESC cultures from E12.5 cortices were treated with Bromodeoxy-Uridine (BrdU) one day before fixation to identify NESC divisions. BrdU+

daughter pairs were classified as one of the three different division types using Nestin (white) and Tubb3 (red).

(D) The increased proportion of neurogenic symmetric divisions was still observed when the *Kif20b* mutant was combined with p53 knockout (*Kif20b-/-; p53-/-),* but was not seen in controls: double heterozygotes (*Kif20b+/-; p53+/-*) or p53 single mutants (*Kif20b+/-; p53-/-*). N=276 control (*Kif20b+/-; p53+/-*) division pairs (3 brains), 228 *p53* single mutant (*Kif20b+/-; p53-/-*) division pairs (3 brains), and 270 double mutant (*Kif20b-/-; p53-/-*) division pairs (5 brains).

(E) Cell cycle exit among the daughters of NESC division pairs was scored as daughters that were BrdU+, Tubb3+. The increased cell cycle exit in *Kif20b*-/- daughters is not dependent on p53 function.

n= 613 control (*Kif20b+/-; p53+/-*) daughter cells; 689 p53 single mutant daughters (*Kif20b+/-; p53-/-*); and 593 double mutant daughter cells (*Kif20b-/-; p53-/-*).

**** p<0.0001, *** p<0.001, ** p<0.01, * p<0.05, n.s. not significant; χ^2 for populations in A, B, D, E, and Fisher's exact test for individual groups in A and B.

Scale bar, 10μm.

References

Abaza, A., J.M. Soleilhac, J. Westendorf, M. Piel, I. Crevel, A. Roux, and F. Pirollet. 2003. M phase phosphoprotein 1 is a human plus-end-directed kinesin-related protein required for cytokinesis. *J Biol Chem*. 278:27844-27852.

Bastos, R.N., and F.A. Barr. 2010. Plk1 negatively regulates Cep55 recruitment to the midbody to ensure orderly abscission. *The Journal of cell biology*. 191:751-760.

Bernabe-Rubio, M., G. Andres, J. Casares-Arias, J. Fernandez-Barrera, L. Rangel, N. Reglero-Real, D.C. Gershlick, J.J. Fernandez, J. Millan, I. Correas, D.G. Miguez, and M.A.

Alonso. 2016. Novel role for the midbody in primary ciliogenesis by polarized epithelial cells. *The Journal of cell biology*. 214:259-273.

Bizzotto, S., and F. Francis. 2015. Morphological and functional aspects of progenitors perturbed in cortical malformations. *Frontiers in cellular neuroscience*. 9:30.

Bondeson, M.L., K. Ericson, S. Gudmundsson, A. Ameur, F. Ponten, J. Wesstrom, C. Frykholm, and M. Wilbe. 2017. A nonsense mutation in CEP55 defines a new locus for a Meckel-like syndrome, an autosomal recessive lethal fetal ciliopathy. *Clin Genet*.

Bowen, M.E., J. McClendon, H.K. Long, A. Sorayya, J.L. Van Nostrand, J. Wysocka, and L.D. Attardi. 2019. The Spatiotemporal Pattern and Intensity of p53 Activation Dictates Phenotypic Diversity in p53-Driven Developmental Syndromes. *Dev Cell*. 50:212-228 e216.

Carlton, J.G., A. Caballe, M. Agromayor, M. Kloc, and J. Martin-Serrano. 2012. ESCRT-III governs the Aurora B-mediated abscission checkpoint through CHMP4C. *Science*. 336:220-225.

Chai, Y., D. Tian, Y. Yang, G. Feng, Z. Cheng, W. Li, and G. Ou. 2012. Apoptotic regulators promote cytokinetic midbody degradation in C. elegans. *The Journal of cell biology*. 199:1047-1055.

Chau, K.F., M.W. Springel, K.G. Broadbelt, H.Y. Park, S. Topal, M.P. Lun, H. Mullan, T. Maynard, H. Steen, A.S. LaMantia, and M.K. Lehtinen. 2015. Progressive Differentiation and Instructive Capacities of Amniotic Fluid and Cerebrospinal Fluid Proteomes following Neural Tube Closure. *Dev Cell*. 35:789-802.

Connell, J.W., C. Lindon, J.P. Luzio, and E. Reid. 2009. Spastin couples microtubule severing to membrane traffic in completion of cytokinesis and secretion. *Traffic*. 10:42-56.

Crowell, E.F., A.L. Gaffuri, B. Gayraud-Morel, S. Tajbakhsh, and A. Echard. 2014. Engulfment of the midbody remnant after cytokinesis in mammalian cells. *J Cell Sci*. 127:3840-3851.

Daniel, E., M. Daude, I. Kolotuev, K. Charish, V. Auld, and R. Le Borgne. 2018. Coordination of Septate Junctions Assembly and Completion of Cytokinesis in Proliferative Epithelial Tissues. *Curr Biol*. 28:1380-1391 e1384.

Di Cunto, F., S. Imarisio, E. Hirsch, V. Broccoli, A. Bulfone, A. Migheli, C. Atzori, E. Turco, R. Triolo, G.P. Dotto, L. Silengo, and F. Altruda. 2000. Defective neurogenesis in citron kinase knockout mice by altered cytokinesis and massive apoptosis. *Neuron*. 28:115-127.

Dionne, L.K., X.J. Wang, and R. Prekeris. 2015. Midbody: from cellular junk to regulator of cell polarity and cell fate. *Curr Opin Cell Biol*. 35:51-58.

Dubreuil, V., A.M. Marzesco, D. Corbeil, W.B. Huttner, and M. Wilsch-Brauninger. 2007. Midbody and primary cilium of neural progenitors release extracellular membrane particles enriched in the stem cell marker prominin-1. *The Journal of cell biology*. 176:483-495.

Dwyer, N.D., B. Chen, S.J. Chou, S. Hippenmeyer, L. Nguyen, and H.T. Ghashghaei. 2016. Neural Stem Cells to Cerebral Cortex: Emerging Mechanisms Regulating Progenitor Behavior and Productivity. *J Neurosci*. 36:11394-11401.

Dwyer, N.D., D.K. Manning, J.L. Moran, R. Mudbhary, M.S. Fleming, C.B. Favero, V.M. Vock, D.D. O'Leary, C.A. Walsh, and D.R. Beier. 2011. A forward genetic screen with a thalamocortical axon reporter mouse yields novel neurodevelopment mutants and a distinct Emx2 mutant phenotype. *Neural Dev*. 6:3.

Elia, N., R. Sougrat, T.A. Spurlin, J.H. Hurley, and J. Lippincott-Schwartz. 2011. Dynamics of endosomal sorting complex required for transport (ESCRT) machinery during cytokinesis and its role in abscission. *Proc Natl Acad Sci U S A*. 108:4846-4851.

Ettinger, A.W., M. Wilsch-Brauninger, A.M. Marzesco, M. Bickle, A. Lohmann, Z. Maliga, J. Karbanova, D. Corbeil, A.A. Hyman, and W.B. Huttner. 2011. Proliferating versus differentiating stem and cancer cells exhibit distinct midbody-release behaviour. *Nat Commun*. 2:503.

Fazeli, G., M. Trinkwalder, L. Irmisch, and A.M. Wehman. 2016. C. elegans midbodies are released, phagocytosed and undergo LC3-dependent degradation independent of macroautophagy. *J Cell Sci*. 129:3721-3731.

Frosk, P., H.H. Arts, J. Philippe, C.S. Gunn, E.L. Brown, B. Chodirker, L. Simard, J. Majewski, S. Fahiminiya, C. Russell, Y.P. Liu, F.C. Consortium, M. Canadian Rare Diseases, N. Mechanisms, R. Hegele, N. Katsanis, C. Goerz, M.R. Del Bigio, and E.E. Davis. 2017. A truncating mutation in CEP55 is the likely cause of MARCH, a novel syndrome affecting neuronal mitosis. *J Med Genet*. 54:490-501.

Gershony, O., S. Sherman, S. Adar, I. Segal, D. Nachmias, I. Goliand, and N. Elia. 2017. Measuring abscission spatiotemporal dynamics using quantitative high-resolution microscopy. *Methods in cell biology*. 137:205-224.

Green, R.A., E. Paluch, and K. Oegema. 2012. Cytokinesis in animal cells. *Annual review of cell and developmental biology*. 28:29-58.

Gromley, A., A. Jurczyk, J. Sillibourne, E. Halilovic, M. Mogensen, I. Groisman, M. Blomberg, and S. Doxsey. 2003. A novel human protein of the maternal centriole is required for the final stages of cytokinesis and entry into S phase. *The Journal of cell biology*. 161:535-545.

Gromley, A., C. Yeaman, J. Rosa, S. Redick, C.T. Chen, S. Mirabelle, M. Guha, J. Sillibourne, and S.J. Doxsey. 2005. Centriolin anchoring of exocyst and SNARE complexes at the midbody is required for secretory-vesicle-mediated abscission. *Cell*. 123:75-87.

Gruneberg, U., R. Neef, X. Li, E.H. Chan, R.B. Chalamalasetty, E.A. Nigg, and F.A. Barr. 2006. KIF14 and citron kinase act together to promote efficient cytokinesis. *The Journal of cell biology*. 172:363-372.

Guizetti, J., L. Schermelleh, J. Mantler, S. Maar, I. Poser, H. Leonhardt, T. Muller-Reichert, and D.W. Gerlich. 2011. Cortical constriction during abscission involves helices of ESCRT-III-dependent filaments. *Science*. 331:1616-1620.

Hayashi, S., P. Lewis, L. Pevny, and A.P. McMahon. 2002. Efficient gene modulation in mouse epiblast using a Sox2Cre transgenic mouse strain. *Mech Dev*. 119 Suppl 1:S97-S101.

Herszterg, S., D. Pinheiro, and Y. Bellaiche. 2014. A multicellular view of cytokinesis in epithelial tissue. *Trends Cell Biol*. 24:285-293.

Higashi, T., T.R. Arnold, R.E. Stephenson, K.M. Dinshaw, and A.L. Miller. 2016. Maintenance of the Epithelial Barrier and Remodeling of Cell-Cell Junctions during Cytokinesis. *Curr Biol*. 26:1829-1842.

Jacks, T., L. Remington, B.O. Williams, E.M. Schmitt, S. Halachmi, R.T. Bronson, and R.A. Weinberg. 1994. Tumor spectrum analysis in p53-mutant mice. *Curr Biol*. 4:1-7.

Janisch, K.M., and N.D. Dwyer. 2016. Imaging and quantitative analysis of cytokinesis in developing brains of Kinesin-6 mutant mice. *Methods in cell biology*. 131:233-252.

Janisch, K.M., K.C. McNeely, J.M. Dardick, S.H. Lim, and N.D. Dwyer. 2018. Kinesin-6 KIF20B is required for efficient cytokinetic furrowing and timely abscission in human cells. *Mol Biol Cell*. 29:166-179.

Janisch, K.M., V.M. Vock, M.S. Fleming, A. Shrestha, C.M. Grimsley-Myers, B.A. Rasoul, S.A. Neale, T.D. Cupp, J.M. Kinchen, K.F. Liem, Jr., and N.D. Dwyer. 2013. The vertebrate-specific Kinesin-6, Kif20b, is required for normal cytokinesis of polarized cortical stem cells and cerebral cortex size. *Development*. 140:4672-4682.

Kim, S., M.K. Lehtinen, A. Sessa, M.W. Zappaterra, S.H. Cho, D. Gonzalez, B. Boggan, C.A. Austin, J. Wijnholds, M.J. Gambello, J. Malicki, A.S. LaMantia, V. Broccoli, and C.A. Walsh. 2010. The apical complex couples cell fate and cell survival to cerebral cortical development. *Neuron*. 66:69-84.

Konig, J., E.B. Frankel, A. Audhya, and T. Muller-Reichert. 2017. Membrane remodeling during embryonic abscission in Caenorhabditis elegans. *The Journal of cell biology*. 216:1277-1286.

Kuo, T.C., C.T. Chen, D. Baron, T.T. Onder, S. Loewer, S. Almeida, C.M. Weismann, P. Xu, J.M. Houghton, F.B. Gao, G.Q. Daley, and S. Doxsey. 2011. Midbody accumulation through evasion of autophagy contributes to cellular reprogramming and tumorigenicity. *Nat Cell Biol*. 13:1214-1223.

Lafaurie-Janvore, J., P. Maiuri, I. Wang, M. Pinot, J.B. Manneville, T. Betz, M. Balland, and M. Piel. 2013. ESCRT-III assembly and cytokinetic abscission are induced by tension release in the intercellular bridge. *Science*. 339:1625-1629.

Lambrus, B.G., V. Daggubati, Y. Uetake, P.M. Scott, K.M. Clutario, G. Sluder, and A.J. Holland. 2016. A USP28-53BP1-p53-p21 signaling axis arrests growth after centrosome loss or prolonged mitosis. *The Journal of cell biology*. 214:143-153.

Lenhart, K.F., and S. DiNardo. 2015. Somatic cell encystment promotes abscission in germline stem cells following a regulated block in cytokinesis. *Dev Cell*. 34:192-205.

Li, H., S.L. Bielas, M.S. Zaki, S. Ismail, D. Farfara, K. Um, R.O. Rosti, E.C. Scott, S. Tu, N.C. Chi, S. Gabriel, E.Z. Erson-Omay, A.G. Ercan-Sencicek, K. Yasuno, A.O. Caglayan, H. Kaymakcalan, B. Ekici, K. Bilguvar, M. Gunel, and J.G. Gleeson. 2016. Biallelic Mutations in Citron Kinase Link Mitotic Cytokinesis to Human Primary Microcephaly. *Am J Hum Genet*. 99:501-510.

Little, J.N., and N.D. Dwyer. 2019. p53 deletion rescues lethal microcephaly in a mouse model with neural stem cell abscission defects. *Hum Mol Genet*. 28:434-447.

Meitinger, F., J.V. Anzola, M. Kaulich, A. Richardson, J.D. Stender, C. Benner, C.K. Glass, S.F. Dowdy, A. Desai, A.K. Shiau, and K. Oegema. 2016. 53BP1 and USP28 mediate p53 activation and G1 arrest after centrosome loss or extended mitotic duration. *The Journal of cell biology*. 214:155-166.

Mierzwa, B., and D.W. Gerlich. 2014. Cytokinetic abscission: molecular mechanisms and temporal control. *Dev Cell*. 31:525-538.

Muzumdar, M.D., B. Tasic, K. Miyamichi, L. Li, and L. Luo. 2007. A global double-fluorescent Cre reporter mouse. *Genesis*. 45:593-605.

Nahse, V., L. Christ, H. Stenmark, and C. Campsteijn. 2017. The Abscission Checkpoint: Making It to the Final Cut. *Trends Cell Biol*. 27:1-11.

Paridaen, J.T., and W.B. Huttner. 2014. Neurogenesis during development of the vertebrate central nervous system. *EMBO Rep*. 15:351-364.

Peterman, E., P. Gibieza, J. Schafer, V.A. Skeberdis, A. Kaupinis, M. Valius, X. Heiligenstein, I. Hurbain, G. Raposo, and R. Prekeris. 2019. The post-abscission midbody is an intracellular signaling organelle that regulates cell proliferation. *Nat Commun*. 10:3181.

Pilaz, L.J., J.J. McMahon, E.E. Miller, A.L. Lennox, A. Suzuki, E. Salmon, and D.L. Silver. 2016. Prolonged Mitosis of Neural Progenitors Alters Cell Fate in the Developing Brain. *Neuron*. 89:83-99.

Pollarolo, G., J.G. Schulz, S. Munck, and C.G. Dotti. 2011. Cytokinesis remnants define first neuronal asymmetry in vivo. *Nat Neurosci*. 14:1525-1533.

Qian, X., S.K. Goderie, Q. Shen, J.H. Stern, and S. Temple. 1998. Intrinsic programs of patterned cell lineages in isolated vertebrate CNS ventricular zone cells. *Development*. 125:3143-3152.

Salzmann, V., C. Chen, C.Y. Chiang, A. Tiyaboonchai, M. Mayer, and Y.M. Yamashita. 2014. Centrosome-dependent asymmetric inheritance of the midbody ring in Drosophila germline stem cell division. *Mol Biol Cell*. 25:267-275.

Singh, D., and C. Pohl. 2014. A function for the midbody remnant in embryonic patterning. *Commun Integr Biol*. 7:e28533.

Skop, A.R., H. Liu, J. Yates, 3rd, B.J. Meyer, and R. Heald. 2004. Dissection of the mammalian midbody proteome reveals conserved cytokinesis mechanisms. *Science*. 305:61-66.

Steigemann, P., C. Wurzenberger, M.H. Schmitz, M. Held, J. Guizetti, S. Maar, and D.W. Gerlich. 2009. Aurora B-mediated abscission checkpoint protects against tetraploidization. *Cell*. 136:473-484.

Stoten, C.L., and J.G. Carlton. 2018. ESCRT-dependent control of membrane remodelling during cell division. *Semin Cell Dev Biol*. 74:50-65.

Figure 1: Asymmetric furrow ingression in control and *Kif20b* mutant NESCs.

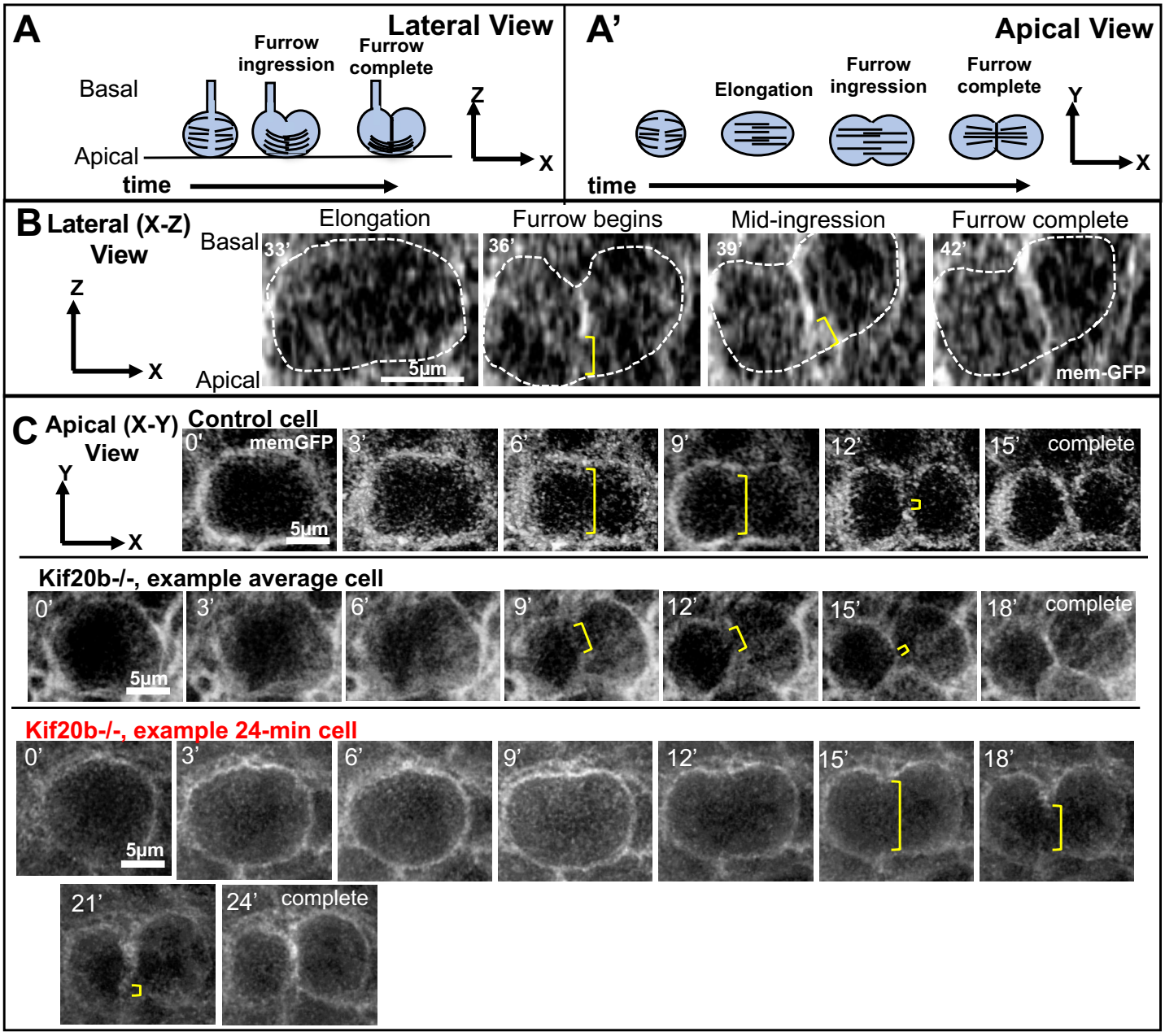

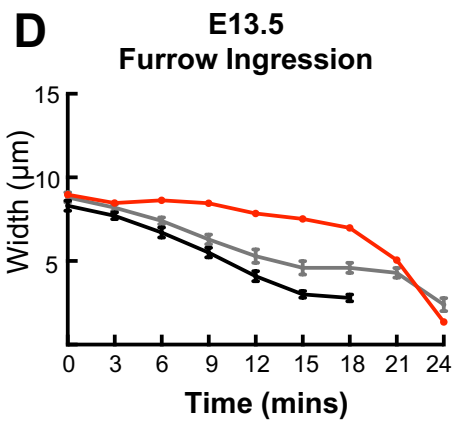

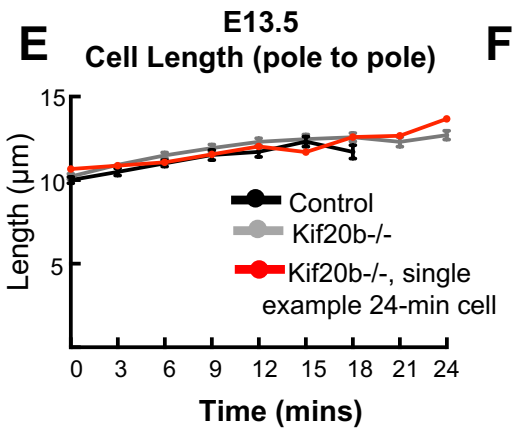

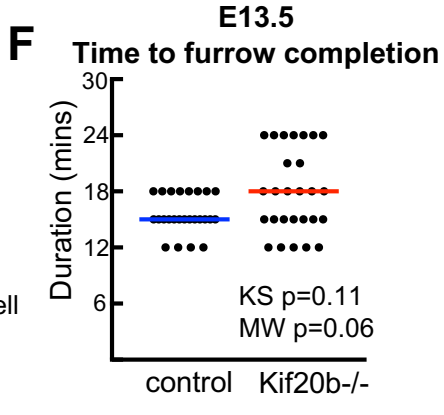

Figure 2: Abscission in NESCs is variable in duration but accelerated in *Kif20b* mutant brains.

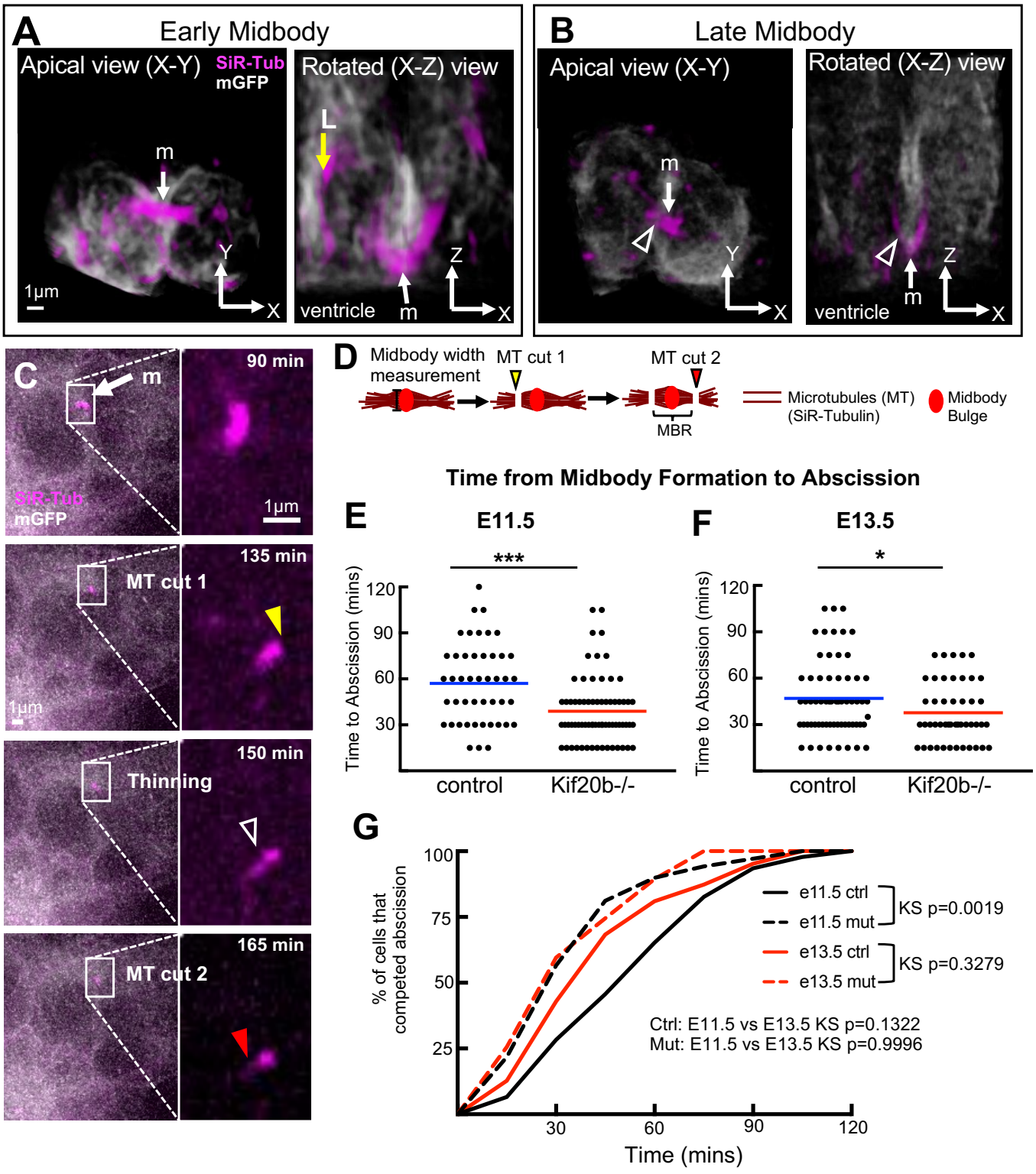

Figure 3: Sequential bilateral abscissions are observed in most NESC divisions, and occur faster in *Kif20b* -/- brains.

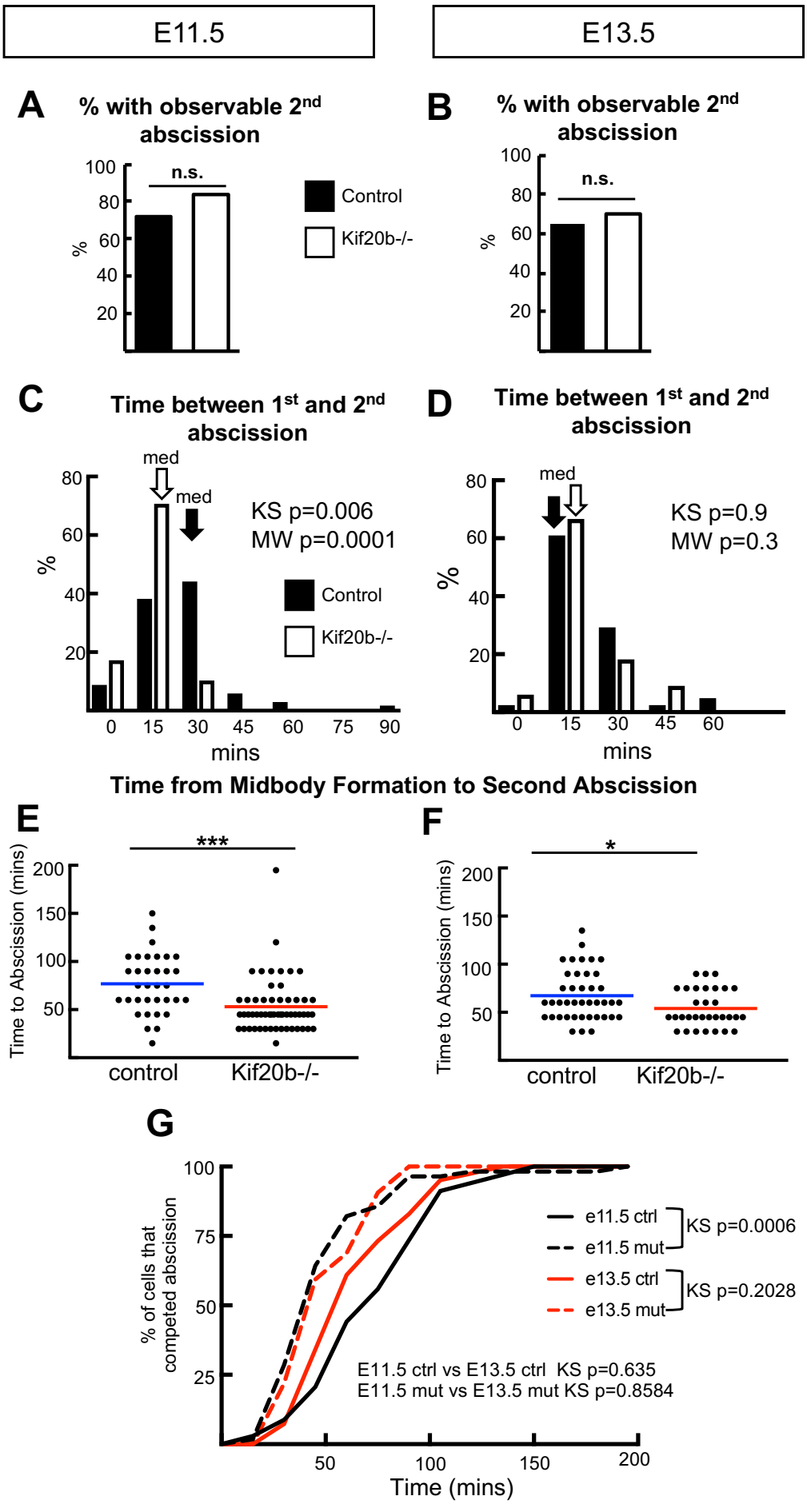

Figure 4: Post-abscission midbody remnants (MBR) are detected at the apical membrane, and associated with early proliferative symmetric divisions.

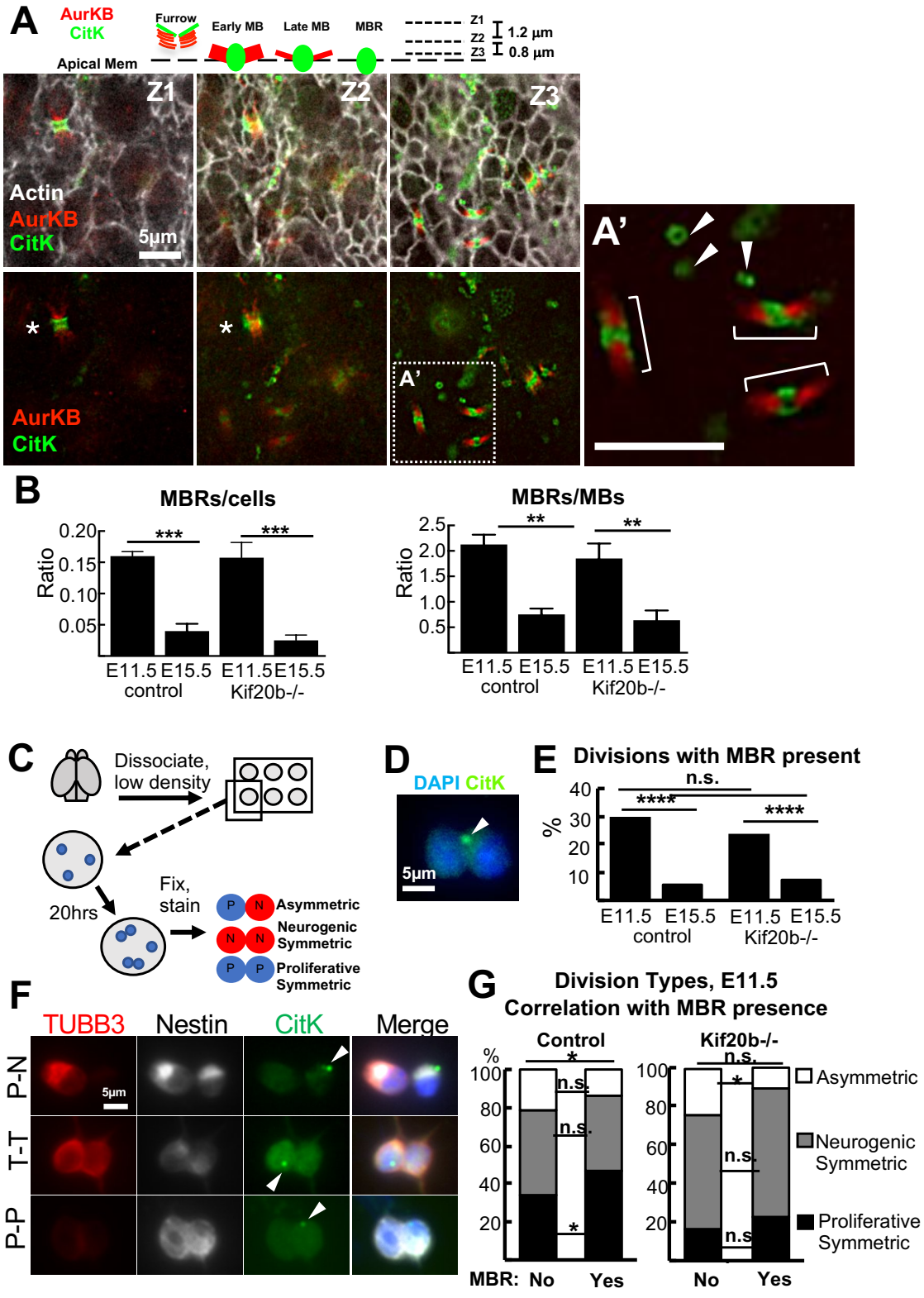

Figure 5: *Kif20b* -/- NESCs show reduced proliferative symmetric divisions and increased neuron daughters in early corticogenesis.

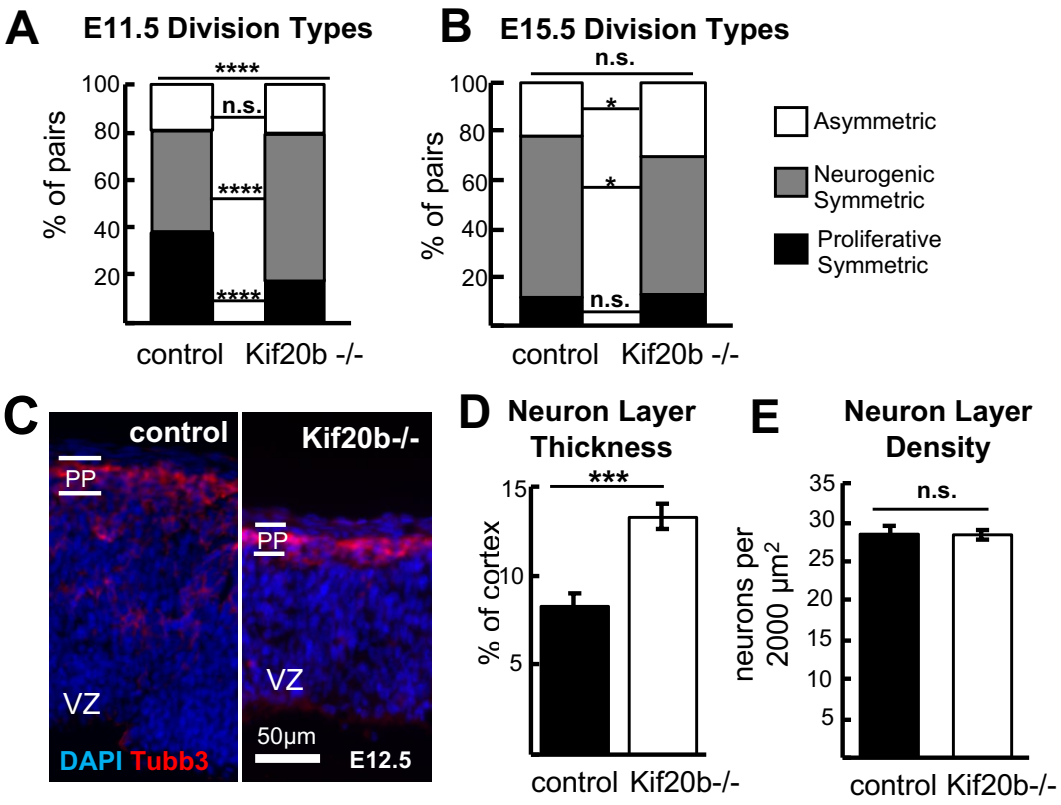

Supplemental Figure 1: Supplemental analyses of furrowing kinetics at E11.5 and midbody width at abscission

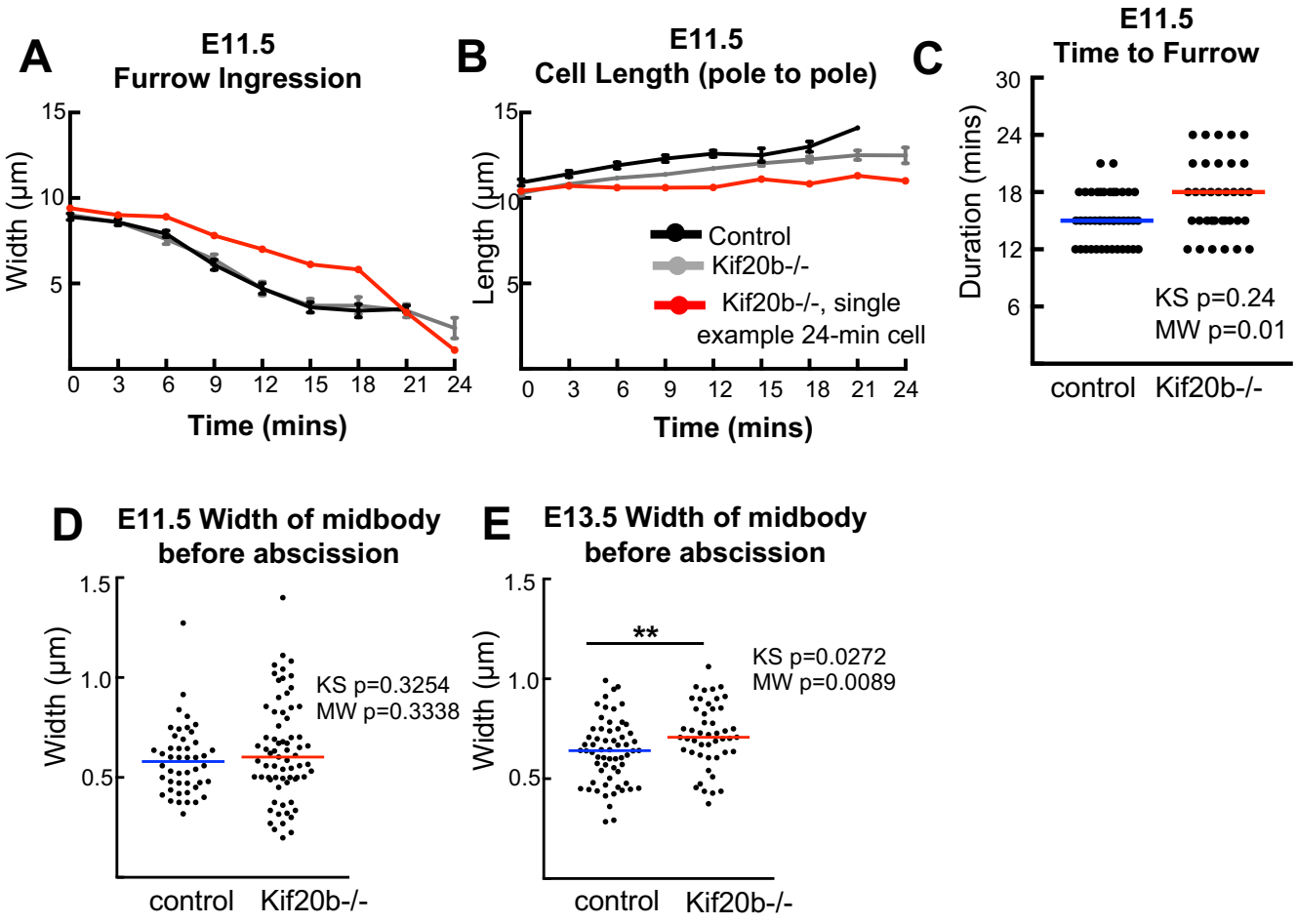

Supplemental Figure 2: NESC midbody remnants (MBRs) are marked by Citron Kinase (CitK) and Cep55.

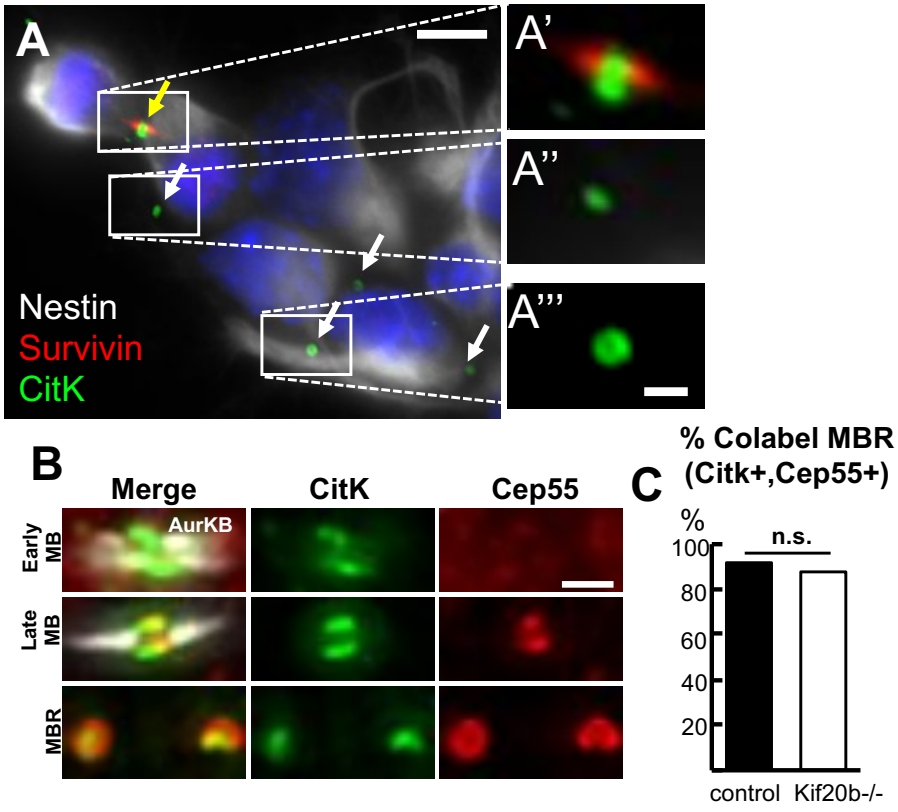

Supplemental Figure 3: The increased neuronal fate of *Kif20b* mutant NESC daughters during early cortical development is not p53-dependent.